ChemPubSoc Europe
DOI: 10.1002/ejic.201900387
EurJIC European Journal of Inorganic Chemistry
Full Paper

Bimodal Contrast Agents | *Very Important Paper* |

Bimodal Probe for Magnetic Resonance Imaging and Photoacoustic Imaging Based on a PCTA-Derived Gadolinium(III) Complex and ZW800–1

Marie Devreux,[a] Céline Henoumont,[a] Fabienne Dioury,[b] Dimitri Stanicki,[a] Sébastien Boutry,[c] Lionel Larbanoix,[c] Clotilde Ferroud,[b] Robert N. Muller,[a,c] and Sophie Laurent*[a,c]

Abstract: One of the most widely used techniques to obtain anatomical information is magnetic resonance imaging (MRI). Despite its high resolution, it has a low sensitivity which could be enhanced by coupling MRI with a more sensitive technique such as photoacoustic imaging (PAI). The development of a bimodal agent could thus lead to hybrid images with a high anatomical resolution provided by MRI and a precise localization of the contrast agent thanks to PAI. The probes used in this work are a gadolinium(III) complex derived from PCTA-[12] for MRI and the ZW800–1 fluorophore for PAI. These two organic parts have been attached to a *L*-lysine derivative which has a third site for potential conjugation to a biovector, thus opening the field of targeted probes for molecular imaging. Preliminary relaxometric and photoacoustic characterizations indicate that this bimodal agent is a promising compound for bimodal imaging.

1. Introduction

Medical imaging plays a major role in medicine to facilitate diagnosis. One of the most widely used techniques is magnetic resonance imaging (MRI) because it has a high spatial resolution (10 μm – 1 mm) and is non-invasive, based on the detection of water protons naturally present in the body.[1] However, MRI is a non-sensitive technique (ca. 100 μM) and requires in some cases the use of a paramagnetic contrast agent (CA), most often being a gadolinium(III) chelate, that reduces the relaxation times of protons present in its vicinity and consequently increases the contrast in the regions where it is located. However, since the gadolinium ion is toxic in its free form, it has to be injected as a complex characterized by a high kinetic inertness and a good thermodynamic stability in order to prevent the Gd(III) release into the body. The injectable dose of CA is quite high (approximately 0.1 mmol/kg) which can be problematic for people with kidney failure who could develop nephrogenic systemic fibrosis due to a slow elimination of the gadolinium complex and the liberation of free gadolinium ions, as described previously.[2] Moreover, new researches have shown the presence of gadolinium in the brain of the patients after several injections.[3] In such cases, an alternative could be to use a bimodal system where MRI would be combined with a more sensitive technique thus enabling to reduce the quantities of gadolinated species injected.

The concept of bimodal probe is very interesting because both modalities can be performed with a single injection for the patient. In the literature, there are different bimodal contrast agents, the most common combination of which is MRI, for its high spatial resolution, associated with another technique that can provide more information. The second modality is generally a more sensitive technique, such as PET, or optical imaging. To implement this model, different types of bimodal structures can be used such as dendrimers, liposomes, nanoparticles, or small organic molecules.[4–6] In this work, we decided to combine MRI with photoacoustic imaging (PAI), a quite new technique in biomedical imaging. PAI is based on the excitation of endogenous or exogenous molecules by a pulsed laser, followed by the detection of pressure waves resulting from the heat produced by the de-excitation. Heat is detected as pressure waves produced by the dilatation of the surrounding tissues, thus allowing images to be reconstructed.[8–10]

Despite a lower spatial resolution (75 μm) than MRI, PAI would provide additional information since its sensitivity is higher (ca. 100 pM). Moreover, PAI is a noninvasive technique with a penetration depth limited up to 4 cm which is suitable for preclinical studies in mice and rats but limiting the applications in the clinical field to surface diseases such as skin cancers.

[a] *NMR and Molecular Imaging, University of Mons, 19 Avenue Maistriau, 7000 Mons, Belgium*
E-mail: sophie.laurent@umons.ac.be
[b] *Laboratoire de Génomique, Bioinformatique et Chimie Moléculaire, EA 7528, Conservatoire National des Arts et Métiers, HESAM Université, 2 rue Conté, 75003 Paris, France*
[c] *Center of Microscopy and Molecular Imaging, 8 rue Adrienne Bolland, 6041 Charleroi, Belgium*

Author contributions: *Conceived and designed the experiments: S. L., C. H., F. D., D. S. Performed the experiments: M. D., C. H., L. L., S. B. Analyzed data: M. D., C. H., L. L., S. B. Contributed reagents/analysis tools/materials: S. L., R. N. M., C. F. Wrote the paper: M. D., C. H., F. D., D. S., L. L., S. B., S. L., C. F. All authors read and approved the final manuscript.*
Supporting information and ORCID(s) from the author(s) for this article are available on the WWW under https://doi.org/10.1002/ejic.201900387.

The combination of the two modalities therefore appears to be a good solution to compensate for the weaknesses of each one of them, especially for preclinical studies. In the literature, only few researches can be found on this combination, all involving nanoparticulate structures.[7] Allowing more favorable pharmacokinetic properties than nanoparticles and faster elimination by kidney, an approach based on the use of a small organic molecule was chosen here, even if the ratio 1:1 of the two modalities seems not favorable considering the difference of sensitivity between the two techniques.[6,7,11] This can be rationalized by the fact that MRI and PAI images cannot be recorded simultaneously, so that MRI scan could be performed at first, and followed by the PAI one during which a part of the agent would be eliminated from the body through the kidneys. It is also important to mention that, considering the limited penetration depth of PAI, this agent is at first dedicated to preclinical studies for which the PAI probe will allow a more precise detection of the targeted disease in the context of molecular imaging.

Most of the agents for MRI are based on 1,4,7,10-tetraazacyclododecane-1,4,7,10-tetraacetic acid (DOTA), which can form an eight-coordinated complex with gadolinium(III) with one coordinated water molecule. In this work, we decided to use a rigidified analogue based on pyclen framework: the 3,6,9,15-tetraazabicyclo[9.3.1]pentadeca-1(15),11,13-triene-3,6,9-triacetic acid (PCTA-[12], Figure 1).[12] PCTA-[12] has a lower denticity than DOTA so that the resulting gadolinium(III) complex can coordinate two water molecules in its inner-sphere.[13,14] This extended hydration number results in an increased relaxivity (at 20 MHz and 37 °C, r_1 = 5.4 mM^{-1} s^{-1} for Gd-PCTA-[12] compared to 3.5 mM^{-1} s^{-1} for Gd-DOTA). Despite its slightly lower thermodynamic stability (log K is 20.4 for Gd-PCTA-[12], and 24.0 for Gd-DOTA), its faster complex formation, its satisfactory kinetic inertness as well as its in vivo-stability, make Gd-PCTA-[12] an interesting alternative to Gd-DOTA.[14–18] As proof of this valuable coordinating cage, P03277, a Gd-PCTA-[12] derivative, demonstrated a better tumor detection than a standard extracellular contrast agent (gadobutrol) and is currently undergoing human clinical trials.[19,22]

ZW800–1 (Figure 2), the contrastophore chosen for PAI is an organic dye which is a derivative of indocyanine green (ICG) that absorbs in near-infrared (762 nm). This choice was guided to avoid noise resulting from the absorption of endogenous molecules such as hemoglobin, and melanin.[8–10]

The linker chosen to connect the two parts for imaging modalities is *L*-lysine. Indeed, this natural amino acid acts as a tri-

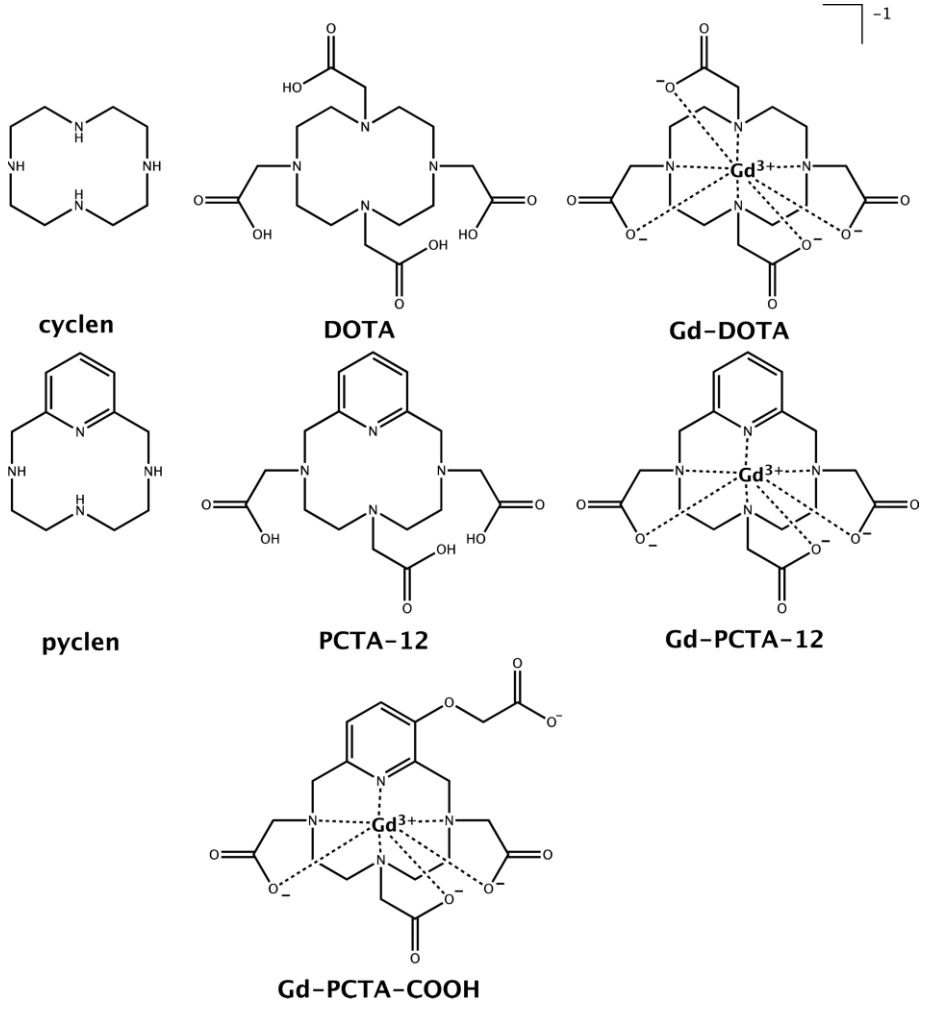

Figure 1. Structures of 12-membered azamacrocycles, acetate N-functionalized polyazamacrocyclic ligands for Gd(III), and the corresponding Gd complexes.

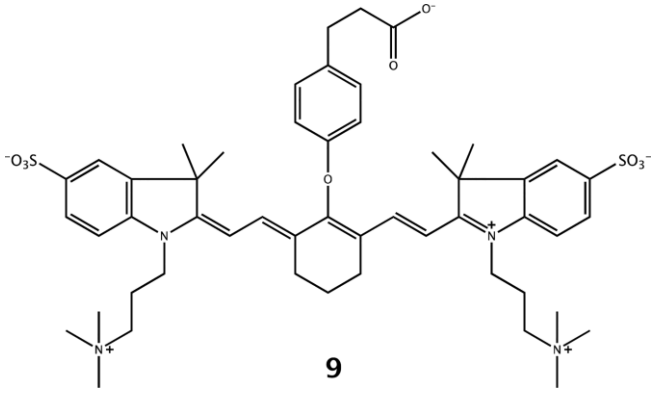

Figure 2. Structure of the PAI probe ZW800–1.

functionalizable platform with two amine and one carboxylic acid functions as potential sites for successive coupling steps. Two of these groups will thus allow the grafting of the two contrastophores, while the third one will remain free for conjugation to a biovector thus making the probe specific to a pathological tissue.

2. Results and Discussion

2.1 Synthesis of the Two Parts of the Bimodal Probe

2.1.1 PCTA(CO_2tBu)$_3$-COOH for MRI (Part 1)

We previously reported the synthesis of PCTA(CO_2tBu)$_3$-COOH,[23,24,26] as a precursor of a bifunctional derivative of PCTA-[12] bearing an additional carboxylic acid function anchored to the pyridine subunit that led to the corresponding Gd-PCTA-COOH chelate for application to the synthesis of targeted Gd-based CA (Figure 1). As previously discussed by us and other,[20,21,25] the preferred synthetic route to PCTA-(CO_2tBu)$_3$-COOH was based on the assembly of two units bearing the final desired functionalities as it allows easier modulation of the nature and number of coordinating sites while avoiding post-macrocyclization functionalization steps with boring selectivity control. Herein, we described optimized protocols to produce higher quantities of this key synthon that is precursor of a variety of PCTA-based bifunctional chelators (BFC). The synthetic pathway involves a controlled macroring step performed by assembling pyridine unit **3** and triamine **6b** (Scheme 1).

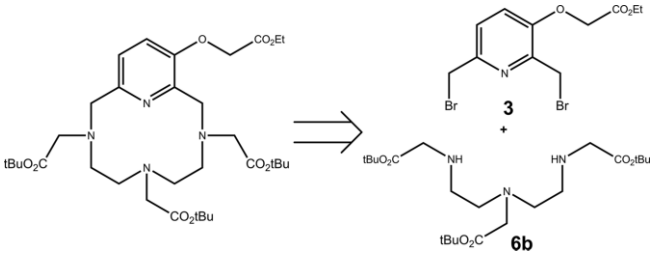

Scheme 1. Retrosynthesis to obtain PCTA(CO_2tBu)$_3$-COOH as precursor of a bifunctional chelating agent for Gd(III).

Compound **3** was prepared from 3-hydroxypyridine with a revised protocol as the three steps/two-pots synthetic route we previously described did not allow us to produce this synthon at tens of grams scale (Scheme 2).[23,26] The first intermediate **1a** (hydrochloric salt) was produced at some forty grams scale with a repeatable average yield of 74 % according to Baldo's protocol.[27] The selective *O*-alkylation of the aromatic hydroxyl proceeded on the corresponding potassium pyridolate **1b** resulting from the treatment of an ethanolic solution of hydrochloride **1a** with an excess of K_2CO_3.[28] The desired dialcohol **2** was obtained by reaction with ethyl bromoacetate in warmed DMF in 65 % yield higher than that previously reported by Hovland et al. for the dodecyloxy analogue.[28] As reported by Uenishi et al. for bipyridine substrates,[29] the Apple reaction with carbon tetrabromide and triphenylphosphane was used to give dibromide **3** in 64 % yield. For this last step, it must be pointed that attempts to proceed in more concentrated medium (0.5 and 1.0 M) were damageable with formation of increasing amounts of a side-product of similar polarity (15 %, and 35 %mol respectively from ^{1}H NMR estimation).

The synthesis of the triamine **6b** starts from the selectively *N,N''*-protected diethylenetriamine derivative **4,**[26] and was optimized as well for the last two steps – tri-*N*-alkylation with *tert*-

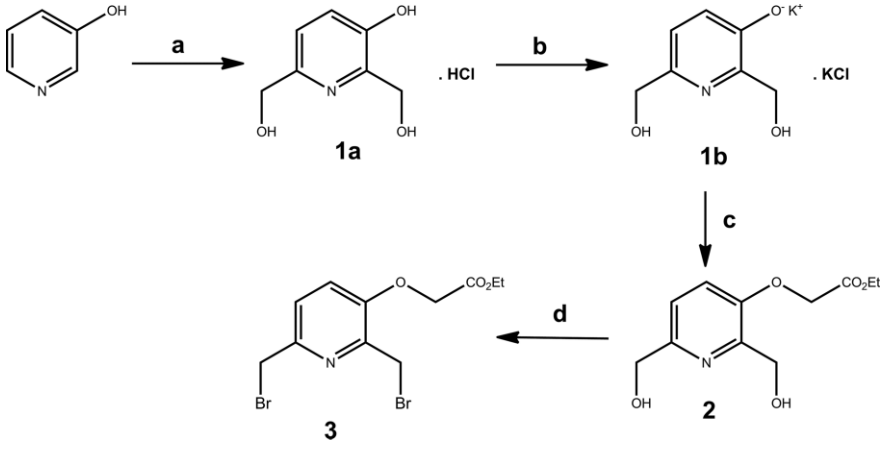

Scheme 2. Synthetic pathway to obtain the pyridine compound **3**. Reagents and conditions: (a) see ref (24); (b) K_2CO_3, EtOH, H_2O, r.t., 3 h; (c) $BrCH_2CO_2Et$, DMF, 80 °C, 1 h30; (d) CBr_4, PPh_3, CH_3CN, 0 °C to r.t., overnight.

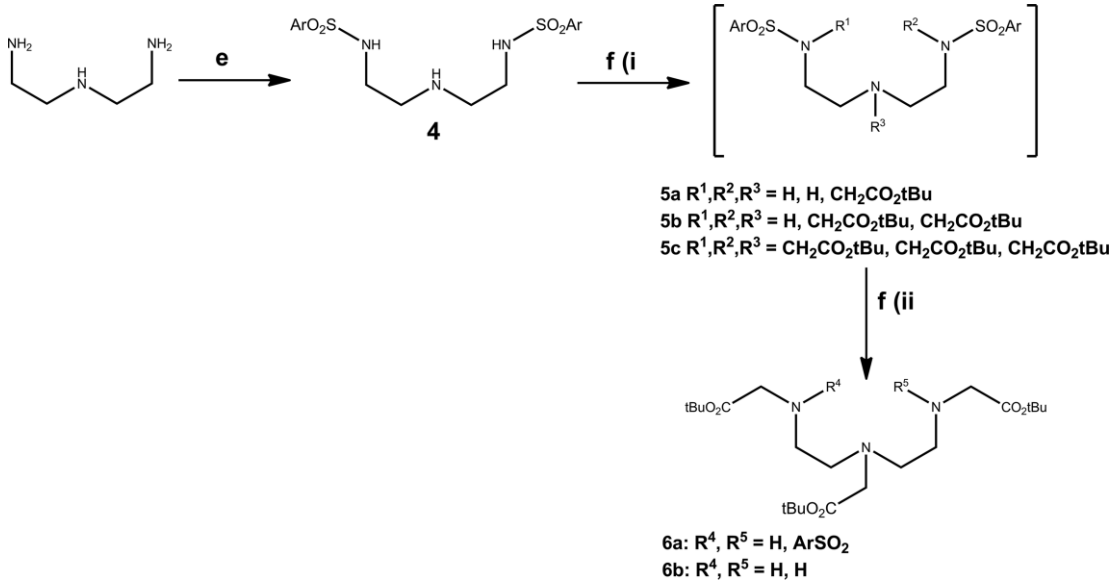

Scheme 3. Synthetic scheme to obtain the triamine **6b.** Reagents and conditions: (e) 2-NO_2-C_6H_4-SO_2Cl, NaOH, Et_2O, THF, H_2O; (f) i) $BrCH_2CO_2tBu$, K_2CO_3, CH_3CN, reflux, 3–5 h; ii) PhSH, K_2CO_3, 60 °C, 2–4 h.

butyl bromoacetate, then selective cleavage of sulfonamidic protections – rendered sequential in one-pot (Scheme 3). In the present work, both steps proceeded in warmed acetonitrile in the presence of K_2CO_3, and afforded synthon **6b** in repeatable 72 % mean yield at scales of more than ten grams. For that protocol, successive monitoring (mass spectroscopy) of the conversion of the intermediates **5a–b** into **5c**, then from **5c** and **6a** into the desired compound **6b** were performed to avoid extending reaction times, particularly that for the second step, thus limiting the formation of the more polar lactamized side-product as reported before.[20] Our pathway constitutes an interesting alternative to that recently reported by C. Picard et al.[25] that involves benzylic protections whose cleavage required pressure of dihydrogen that may be limiting for scaling-up.

The two previously prepared units **3** and **6b** were then assembled on the basis of a recent published macroring process conducted in a diluted medium (reactants concentration 0.002 M) in rather "hard" conditions (refluxing acetonitrile for 2 days with a large excess of sodium carbonate) that gave access to small batches of only a few hundred milligrams.[25] The protocol was revised in the perspective of larger scales. We recently reported a new protocol involving equimolar amounts of compounds **3** and **6b** occurring in DMF in more concentrated medium (reactants concentration 0.01 M) at room temperature for 1 day in the presence of a smaller excess of sodium carbonate that led to the desired macrocycle **7** in 76 % yield for a gram scale.[26] Herein, we found that replacing DMF by acetonitrile, a safer and more easily removable solvent, had no impact on efficiency of the macroring process: larger batches of several grams of compound **7** were obtained with yields above 70 % (Scheme 4). At this stage, a specific spectral feature must be highlighted as the complexity of the ^1H NMR spectrum of the chromatographed material could be disappointing and lead to an erroneous conclusion about the efficiency of the process. Indeed, under milder conditions (lower excess of sodium carbonate, reaction conducted at room temperature), compound **7** was isolated as a mixture of two forms easily distinguished by NMR (Figure 3 and S1):

i) a NaBr adduct as evidenced by the elemental analysis, and in accordance with Na^+ species reported for such derivatives.[25] This NaBr adduct is characterized by a ^1H NMR trace with sharp signals where the methylenic protons in the 3–5 ppm region are split into AB patterns which indicates a stable form in solu-

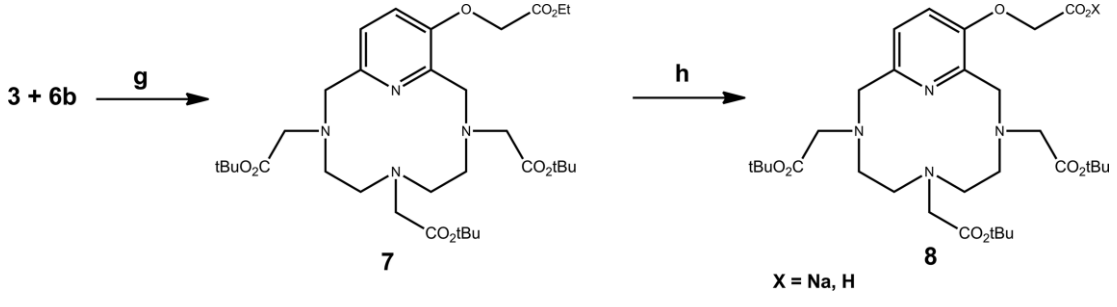

Scheme 4. Synthesis of the precursor of the PCTA-based chelating agent. Reagents and conditions: (g) Na_2CO_3, CH_3CN, r.t., 2 d; (h) NaOH, EtOH, H_2O, r.t., 1 h30.

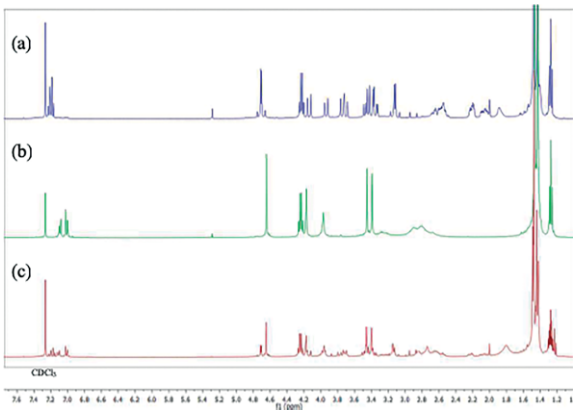

Figure 3. ^{1}H NMR spectra for compound **7**: (a) NaBr adduct; (b) free-Na form; (c) mixture of the two forms.

tion without fluxional behavior at the NMR timescale (Figure 3 (a)). The corresponding ^{13}C NMR spectrum is readily assignable as well (Figure S1 (a));

ii) and a "free-Na" form characterized by an ^{1}H NMR trace with a strong line-broadening for all the CH_2 resonances in the 2.5–4.5 ppm region (Figure 3 (b)). This can be rationalized by the presence of several protonated species in equilibrium due to the four nitrogen atoms of the pyclen framework, and particularly to that of the less basic pyridine subunit. Changes are visible as well on the ^{13}C NMR trace (Figure S1 (b)).

These results corroborate with calculated species distributions (Chemicalize® online platform): at $pH \geq 8$, a single neutral form may exist, while at neutral pH ($6 \leq pH \leq 7$), a mixture of +1-charged species in equilibrium, and of the neutral species may exist. These mixtures were obtained after purification by chromatography. Treatment of a solution of NaBr adduct with basic aluminum oxide induced partial Na dissociation as well; an example of ^{1}H NMR trace for the resulting mixture of the two forms is presented on Figure 3 (c).

The last step of this synthetic route was a selective cleavage of the masked carboxylic acid appended on the pyridine subunit. The corresponding ethyl ester was saponified in mild conditions, by action of a stoichiometric amount of sodium hydroxide in ethanolic solution at room temperature and afforded the desired conjugable prochelator **8** in quantitative yield. As expected, the NMR trace for compound **8** is also highly dependent of the *pH* (Figure 4).

2.1.2 ZW800–1 for PAI (Part 2)

The CA for PAI (Figure 2) was synthesized according to the route described by Choi et al.[10] This indocyanine derivative chosen for its absorption wavelength, in the near-infrared that is outside the absorption range of endogenous molecules and tissues, is ideal and allows a better signal/noise ratio. Moreover, this chromophore has a free carboxylic acid function to serve as functional site for subsequent grafting onto the linker.

2.2 Synthesis of the Bimodal Probe

Selective protections of the three functional sites of *L*-lysine were required to serve as a platform on which the two previously prepared imaging parts will be appended, as well as an additional biovector for targeting purposes.

First, the regioselective carboxybenzyl (Cbz) protection of the amine of the lateral chain was performed with 80 % yield according to the protocol described by Balajhy et al. (Scheme 5).[30] The carboxylic acid was then esterified as allyl ester using the thionyl chloride method that proceeds by an in

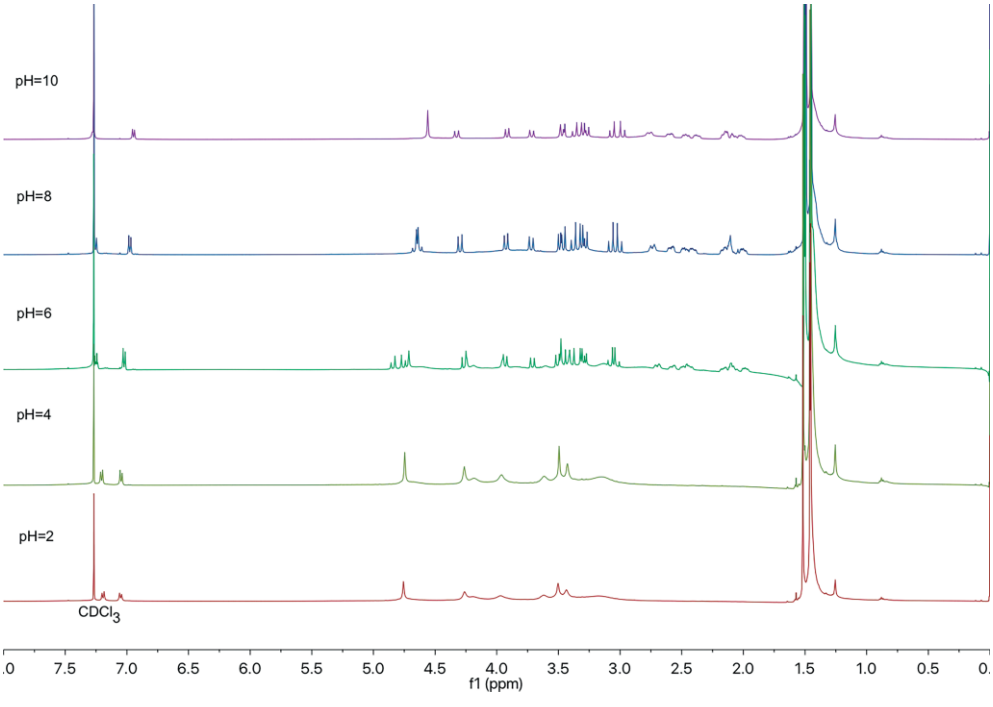

Figure 4. Influence of pH on ^{1}H NMR trace of PCTA(CO_2*t*Bu)$_3$-COOH ($CDCl_3$, 500 MHz).

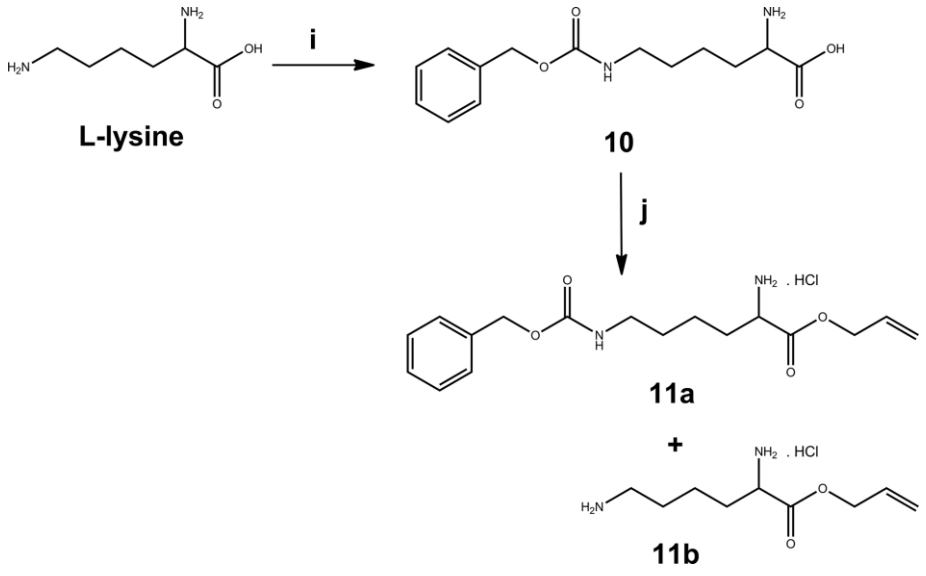

Scheme 5. Preparation of the L-lysine derivative as a trifunctional linker. Reagents and conditions: (i) ref (30); (j) $SOCl_2$, allyl alcohol, reflux, 1 d.

situ activation as acid chloride.[30,31] In such conditions, compound **11a** was obtained with a yield of 46 %. This modest yield can be explained by the instability of the Cbz group in acidic medium evidenced by the formation of H-Lys(H)-OAl **11b** as well. Moreover, this side-product **11b** proved to have a polarity close to that of the desired compound **11a**, and made the chromatographic purification with partial coelution of both products tedious.

The assembling of the two previously prepared parts **8** and **11a** required preliminary optimization (Scheme 6). Different coupling conditions were tested (Table 1). The best results were obtained with hexafluorophosphate *O*-(benzotriazol-1-yl)-*N*,*N*,*N*′,*N*′ tetramethyluronium (HBTU) and with dicyclohexylcarbodiimide/hydroxybenzotriazole (DCC/HOBt) (Entries 2, and 6). The protocol with HBTU was finally preferred as it requires less amount of H-Lys(Cbz)-OAl **11a**, close to the stoichiometry. A treatment with TFA of the resulting PCTA(CO_2*t*Bu)$_3$-Lys(Cbz)-OAl **12** was then done in order to cleave in one-pot the three masked carboxylic acids of the PCTA framework together with the Cbz protection of the pendant linker. This allows to obtain the PCTA-based chelating agent **13** with free carboxylic acid functions able to coordinate a paramagnetic ion, such as the gadolinium ion as an MRI contrast agent. The complexation was performed in water by adding an equimolar amount of gadolinium chloride at a controlled pH between 5 and 6 in order to avoid the precipitation of gadolinium as hydroxides, and afforded the corresponding Gd-chelate **14**.

The last step in this synthesis was to couple Gd-PCTA-Lys(H)-OAl **14** with the fluorophore ZW800–1 **9** (Scheme 7). This was performed with *N*-ethyl-*N*′-(3-dimethylaminopropyl)carbodi-

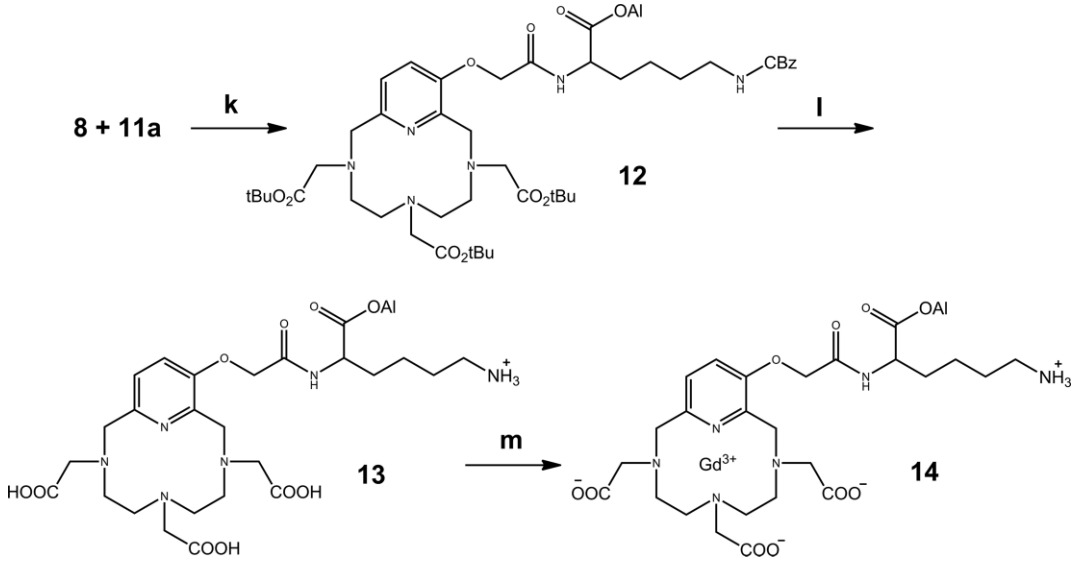

Scheme 6. Preparation of the MRI part of the probe. Reagents and conditions: (k) HBTU, DIPEA, CH_2Cl_2, r.t., 4 h; (l) TFA, CH_2Cl_2, r.t., 3 d; (m) $GdCl_3$, NaOH, water, pH 5–6.

Table 1. Optimization of the coupling reaction between PCTA(CO_2tBu)$_3$-COOH **8** and H-Lys(CBz)-OAl **11a**; all trials were made with ± 100 mg of compound **8** (limiting reagent).

Entry	H-Lys(CBz)-OAl (eq)	Coupling reagent(s)	DIPEA (eq)	Solvent	Yield
1	2.0	EDC•HCl (1.2 equiv.) NHS (1.3 equiv.)	3.3	CH_2Cl_2	0 %
2	2.0	DCC (1.1 equiv.) HOBt•H_2O (0.26 equiv.)	2.0	CH_2Cl_2	34 %
3	2.0	EDC•HCl (1.2 equiv.) HOBt•H_2O (0.26 equiv.)	3.0	CH_2Cl_2	21 %
4	1.5	EDC•HCl (1.2 equiv.) HOBt•H_2O (0.26 equiv.)	3.0	CH_2Cl_2	20 %
5	2.0	EDC•HCl (1.2 equiv.) HOBt•H_2O (0.26 equiv.)	3.0	DMF	9 %
6	1.2	HBTU (2.1 equiv.)	2.4	CH_2Cl_2	38 %

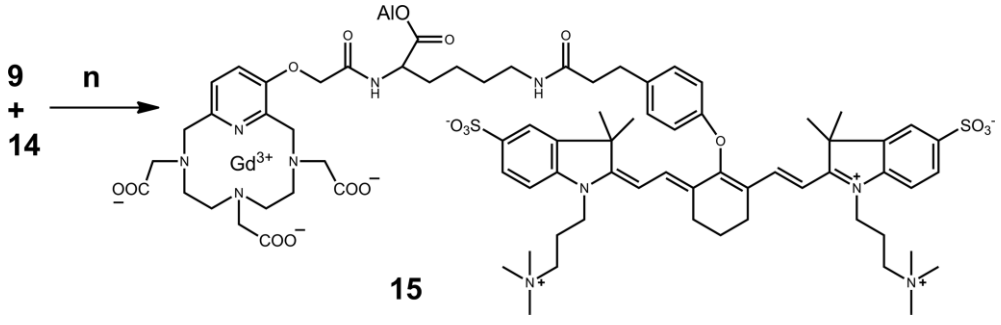

Scheme 7. Dual-modality probe synthesis. Reagents and condition: (n) EDC•HCl, water, pH 5–6.

imide hydrochloride (EDC•HCl) in pH-controlled water to avoid the dissociation of the Gd-chelate. Since an aqueous medium was required to maintain the integrity of the complex, an excess of coupling agent was required to obtain the completion of the reaction. The resulting product **15** was characterized by ESI-TOF MS analysis that shows two characteristic isotopic patterns corresponding to $[M + H]^{2+}$ and $[M + Na]^{2+}$ species consistent with the theoretical simulation (Figure S2). The overall yield obtained for the four last steps is rather low (16 %) but probably increased by further optimization.

2.3 Relaxometric Analysis of the Bimodal Probe

NMRD profiles were recorded for all the Gd complexes (Figure 5). By comparing Gd-PCTA-COOH to Gd-PCTA-Lys(H)-OAl **14**, a damageable effect of the lysine linker grafting on the longitudinal relaxivity r_1 can be deplored. Fortunately, a slightly higher relaxivity was obtained by subsequent grafting of the ZW800–1 fluorophore, with a dependence on the gadolinium concentration. The first verification to explain these results was the determination of the number of water molecules coordinated in the inner-sphere of gadolinium ions. PCTA-(CO_2tBu)$_3$-COOH is a N_4O_3-type heptadentate ligand that allows the presence of two water molecules in the coordination sites of the gadolinium ion.[17] In the present study, the impact of additional functionalization on the number of water molecules was thus measured by ^{17}O NMR. As already described,[32,33] the method consists in measuring the chemical shift difference of the water protons for pure water and for an aqueous solution of the studied gadolinium complex at a known concentration. Comparison with standard solutions of well-known gadolinium complexes allows the determination of the number of inner-sphere water molecules. The comparison with Gd-PCTA-COOH and Gd-DOTA having respectively two and one inner-sphere water molecules allows to deduce that both of the new complexes grafted onto the lysine linker have one water molecule directly coordinated to gadolinium (Figure 6). This is probably due to a new coordination between the carbonyl group on the linker and the gadolinium ion. This result explains the decrease in relaxivity observed for both complexes Gd-PCTA-Lys(H)-OAl **14** and

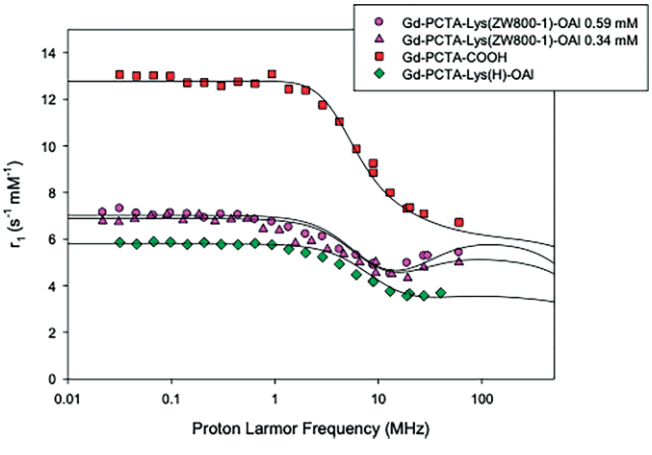

Figure 5. NMRD profiles at 37 °C. The straight lines correspond to the theoretical fitting according to the theory of Solomon and Bloembergen. It has to be noted that the fit at high field (above 100 MHz) is not so reliable considering the partial aggregation of the molecules and is shown here to guide the eyes.

Gd-PCTA-Lys(ZW800–1)-OAl **15**. The relaxivity of Gd-PCTA-Lys(ZW800–1)OAl is nevertheless higher than that of Gd-PCTA-Lys(H)-OAl and depends on the gadolinium concentration, which can probably be explained by the modification of the size of the complex. Each NMRD profile was thus fitted with the Solomon and Bloembergen theory.[34–36] This model predicts that the relaxivity can be modified by different parameters that are: the rotational correlation time τ_R, the electronic relaxation time at zero field τ_{SO}, the correlation time that modulates the electronic relaxation τ_V, the distance between the protons of the coordinated water molecule and the gadolinium (r) and the number of coordinated water molecules (q). The diffusion of water molecules in the vicinity of the gadolinium complex, known as the outer-sphere mechanism, will also influence the relaxivity. It is described by the distance of closest approach between the water molecules and the gadolinium ion (d) and by the relative diffusion coefficient of water (D). This mechanism has however a low and fixed contribution for all gadolinium complexes such that d and D were fixed to 0.36 nm and 3×10^{-9} m^2/s respectively during the fitting. The results of the fitting are presented in Table 2. *r* was fixed at 0.31 nm as described previously, and τ_M was fixed at 100 ns based on the standard evolution of the relaxivity of the small organic complexes without any amide bond with the temperature.[37] The continuous decrease of the relaxivity with increasing temperatures is indeed typical of a fast exchange of the coordinated water molecule, so that 100 ns is an appropriate value.[38] The value of *q* was fixed according to the results obtained by ^{17}O NMR, whereas the other parameters were let to vary. As expected, among those parameters, a modification of the rotational correlation time τ_R is observed for the complex Gd-PCTA-Lys(ZW800–1)-OAl, which can be correlated with the increase of the molecular weight. Moreover, an increase of τ_R is obtained when the concentration of the complex increases, which is probably the sign of a partial aggregation of the molecules by π-stacking, due to the aromatic structure of the ZW800–1.

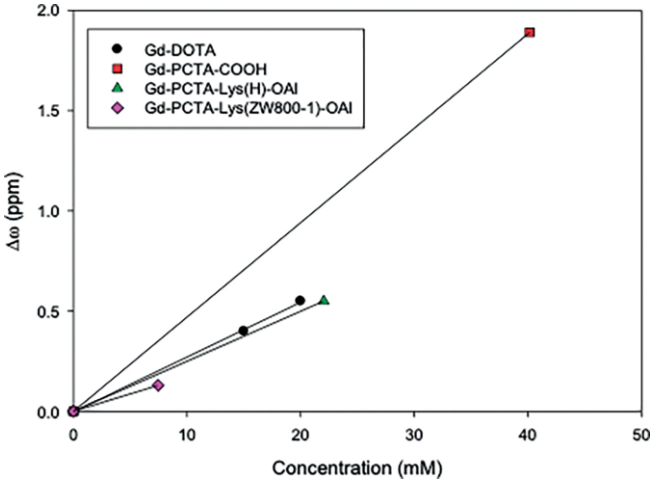

Figure 6. Measurements of the ^{17}O chemical shift of water in the presence of different Gd complexes.

2.4 Phantom Images

As a proof of concept, some phantom images were recorded (Figure 7). The MRI images are compared with Gd-DOTA, a commercially available contrast agent (Dotarem®). As expected according to the previously described physicochemical characterization, the longitudinal relaxation time of water in the presence of Gd-PCTA-Lys(ZW800–1)-OAl **15** (r_1 5.47 mM^{-1} s^{-1}) is shorter than with Gd-DOTA (r_1 2.9 mM^{-1} s^{-1})[40] at 9.4 T, leading to a better contrast. As explained above, this is mostly due to the bigger size of the molecule.

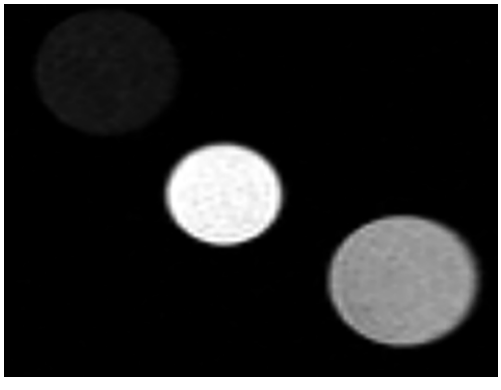

Figure 7. Phantom image at 9.4 T: left: water; middle: Gd-PCTA-Lys(ZW800–1)-OAl **15**; right: Gd-DOTA.

The PAI efficacy of Gd-PCTA-Lys(ZW800–1)-OAl **15** was compared to that of ZW800–1. As shown in Figure 8, the photoac-

Table 2. Parameters extracted from the theoretical fitting of the NMRD profiles according to the Solomon and Bloembergen equations. d, the distance of closest approach and D, the diffusion coefficient of water characterize the outer-sphere contribution to the relaxation; r, the distance between the inner-sphere water molecule and the gadolinium, τ_R, the rotational correlation time, τ_M, the residence time of the coordinated water molecule, τ_{s0}, the Gd(III) electronic relaxation time at zero field and τ_V, the correlation time that modulates the electronic relaxation, define the inner-sphere contribution to the relaxation.

	Gd-PCTA-COOH [b]	Gd-PCTA-Lys(H)-OAl **14**	Gd-PCTA-Lys(ZW800–1)-OAl 0.34 mM **15**	Gd-PCTA-Lys(ZW800–1)-OAl 0.59 mM **15**
d [nm] [a]	0.36	0.36	0.36	0.36
D (m^2 s^{-1}) [a]	3 10^{-9}	3 10^{-9}	3 10^{-9}	3 10^{-9}
r [nm] [a]	0.31	0.31	0.31	0.31
τ_R [ps] [c]	76 ± 1.3	71 ± 19.2	126 ± 20	148 ± 23
τ_M [ns] [a]	100	100	100	100
τ_{s0} [ps] [c]	122 ± 2.2	54 ± 1.7	62.0 ± 1.5	59.0 ± 2.0
τ_V [ps] [c]	45 ± 2.5	9 ± 0.5	12.0 ± 2.0	11.0 ± 1.5
q [a]	2	1	1	1

[a] Fixed parameters during the fitting procedure. [b] The product was prepared according to Guerbet's patent.[39] [c] Obtained by the fitting of NMRD profiles.

oustic signal in the therapeutic range, i.e. in the near infrared (660 nm to 930 nm), is more or less equivalent for Gd-PCTA-Lys(ZW800–1)-OAl **15** and for ZW800–1, the small observed difference being attributed to a small difference in concentration between the two compounds. These results show thus that Gd-PCTA-Lys(ZW800–1)-OAl is a promising bimodal molecule for imaging application.

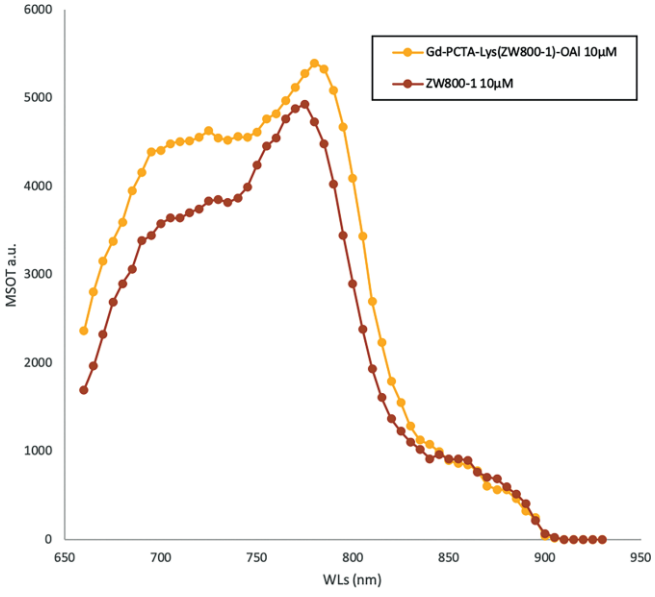

Figure 8. Photoacoustic signal at different wavelengths for *ca* 10 µM solutions of Gd-PCTA-Lys(ZW800–1)-OAl **15** and ZW800–1.

3. Conclusion

The bimodal probe was successfully synthesized, and each intermediate was characterized. The efficiency of this new bimodal probe for MRI and PAI was also assessed. These two imaging techniques could indeed be used jointly in the future to improve the quality of the images with a high spatial resolution provided by MRI and a high sensitivity with optoacoustic imaging. Moreover, we can envision adding a biovector to this probe. Indeed, the linker still possesses a carboxylic acid protected by an allyl group which is available after deprotection to graft, for example, a peptide specific to a biological disorder.

The efficacy of the MRI probe could also be improved by allowing the coordination of two water molecules in the inner-sphere as for the parent compound Gd-PCTA. In that aim, it could be possible to space out the free carboxylic function from the macrocycle in compound **1**. It will be however necessary to verify that the length modification does not change the properties of the bimodal probe.

4. Experimental Section

Materials and Methods

4.1 Chemical and Physical Measurements: All reactions were monitored by mass spectrometry (Waters ZQ2000). Chromatographic purifications were performed on a the Biotage® flash chromatography system using pre-packed cartridges, and automatic fraction collection based on ELSD and/or UV detection (254, and 270 nm). The dialyses were performed on regenerated cellulose membranes from Spectrum labs® characterized by pores of 500 to 1000 Dalton. The elimination of free gadolinium ions was performed with Chelex® 100 resin (sodium form). All synthetic intermediates were characterized by ^{1}H, ^{13}C and COSY NMR (Bruker® AV 400 at 400 MHz, Bruker® Avance II-500 at 500 MHz, Bruker® BioSpin GmbH at 400 MHz or Bruker® NEO at 600 MHz). If not mentioned, spectra were recorded at 298 K. Chemical shifts δ are reported in ppm using the residual deuterated solvent signals as an internal reference ($CDCl_3$: δ_H = 7.26 ppm, δ_C = 77.1 ppm; D_2O: δ_H = 4.80 ppm as internal standard, δ_C = 3-trimethylsilyl-1-propanesulfonic acid sodium salt as external reference; [D_6]DMSO: δ_H = 2.50 ppm, δ_C = 39.5 ppm; CD_3OD: δ_H = 3.31 ppm). For ^{1}H NMR, coupling constants *J* are given in Hz and the resonance multiplicity is described as s (singlet), d (doublet), t (triplet), q (quartet), m (multiplet), and br (broad). The synthetic intermediates were also characterized by mass spectrometry (Waters, ZQ2000 or Synapt G2-*Si*). The relaxometric analyses were performed on Bruker Minispec 20 MHz and 60 MHz and the NMRD profiles were registered on the Stelar Spinmaster (Stelar, Italy). ^{17}O NMR measurements were performed on a Avance II 500 NMR spectrometer (Bruker®) at 37 °C. The photoacoustic measurements were performed on InVision-256TF iThera Medical. The MRI measurements were performed at 9.4 T on Biospec (Bruker®) according to Rapid Acquisition with Relaxation Enhancement sequence (RARE), (TR=350 ms, TE=12 ms, resolution= 156 × 146 microns, slice thickness=1.25 mm, RARE factor=2, 2 or 4 averages).

4.2 Synthesis of the Probe for MRI *PCTA(CO_2tBu)-COOH*, Compound 8

4.2.1 2,6-Bis(hydroxymethyl)pyridin-3-ol, hydrochloride salt, Compound 1a: Compound **1a** (36.7 g, 192 mmol) was prepared from 3-hydroxypyridine (24.0 g, 252 mmol) following the protocol described by Baldo et al.[27]Yields 72–76 % (five repeated trials). Yield 74 % (mean). ^{1}H NMR (D_2O, *pH* 3–4, 400 MHz) δ (ppm): 4.87 (s, 2H); 4.92 (s, 2H); 7.69 (d of AB system, 1H, *J* 8.0 Hz); 7.84 (d of AB system, 1H, *J* 8.0 Hz).

4.2.2 Potassium 2,6-Bis(hydroxymethyl)pyridine-3-olate, Compound 1b: K_2CO_3 (80 g, 579 mmol, 3.0 equiv.) was added to a solution of **1a** (36.7 g, 192 mmol) in ethanol (270 mL) and water (7 mL). The mixture was stirred at room temperature for at least 3 h (stirring can be maintained overnight). Insoluble matter was filtered off, washed with ethanol, and the filtrate was concentrated to dryness to give **1b** (37.0 g, 192 mmol) as a brown oil. Yield 100 %. ^{1}H NMR (D_2O, *pH* 9–10, 400 MHz) δ (ppm): 4.51 (s, 2H); 4.67 (s, 2H); 6.97 (d of AB system, 1H, *J* 8.0 Hz); 7.13 (d of AB system, 1H, *J* 8.0 Hz).

4.2.3 Ethyl 2-{[2,6-Bis(hydroxymethyl)-3-pyridyl]oxy}acetate, Compound 2: Ethyl bromoacetate (22 mL, 199 mmol, 1.5 equiv.) was added to a solution of the crude potassium pyridolate **1b** (26.2 g, 131 mmol) in DMF (100 mL). The mixture was warmed at 80 °C for 1.5 h then maintained in the hot bath cooled to room temperature. Insoluble matter was filtered off, washed with CH_2Cl_2 and the filtrate was concentrated to dryness. The brown oily residue obtained was taken up in CH_2Cl_2 (150 mL) and water (50 mL). The mixture was vigorously stirred then neutralized by portionwise solid $NaHCO_3$ addition. The two layers were separated, and the aqueous layer was extracted with CH_2Cl_2 (2 × 150 mL). The combined organic layers were dried, and concentrated to give a brown oil that was purified by chromatography on silica gel (AcOEt) to afford the desired compound **2** (20.59 g, 85.35 mmol) as a yellow oil that crystallizes on cooling.[23] Yield 65 %. ^{1}H NMR (400 MHz, $CDCl_3$) δ

(ppm): conform to reported data:[15] 1.28 (t, 3H, *J* 7.1 Hz, Et); 4.26 (q, 2H, *J* 7.1 Hz, Et); 4.67 (s, 2H); 4.71 (s, 2H); 4.82 (s, 2H); 7.06 (d of AB system, 1H, *J* 8.4 Hz); 7.19 (d of AB system, 1H, *J* 8.4 Hz).

4.2.4 Ethyl 2-{[2,6-Bis(bromomethyl)-3-pyridyl]oxy}acetate, Compound 3: A solution of the previously prepared pyridinic dihydroxy substrate **2** (4.437 g, 18.39 mmol) in CH_3CN (80 mL) was cooled below 0 °C to add carbon tetrabromide (15.25 g, 46.0 mmol, 2.5 equiv.) in one portion followed by solid triphenylphosphane (12.06 g, 46.0 mmol, 2.5 equiv.) portionwise. After the end of the addition, stirring was maintained overnight in the cold bath allowed to raise up to room temperature. The reaction mixture was concentrated. The brown oil obtained was taken up in CH_2Cl_2 (1000 mL), and washed with a saturated aqueous solution of $NaHCO_3$ (80 mL). The organic phase was dried, and concentrated. The resulting coloured solid was purified by chromatography on silica gel (cyclohexane/AcOEt, 8:2 *v*/*v*) to give the desired compound **3** as a white powder (4.36 g, 11.88 mmol).[23] Yield 64 %. ^{1}H NMR (400 MHz, $CDCl_3$) δ (ppm): conform to reported data:[12] 1.30 (t, 3H, *J* 7.1 Hz, Et); 4.27 (q, 2H, *J* 7.1 Hz, Et); 4.52 (s, 2H); 4.67 (s, 2H); 4.73 (s, 2H); 7.07 (d of AB system, 1H, *J* 8.5 Hz); 7.36 (d of AB system, 1H, *J* 8.5 Hz).

4.2.5 2-Nitro[N(2{2[(2-nitrophenyl)sulfonylamino]ethylamino})-ethyl]benzenesulfonamide, Compound 4: A 2 *M* aqueous solution of sodium hydroxide (56 mL, 112 mmol, 2.0 equiv.) was added to a solution of diethylenetriamine (6.0 mL, 55.54 mmol) in diethyl ether (2 L). The mixture was vigorously stirred at room temperature to add dropwise (in about 2–2.5 h) a solution of 2-nitrophenylsulfonyl chloride (24.61 g, 111 mmol, 2.0 equiv.) in tetrahydrofuran (360 mL). Vigorous stirring was maintained overnight. The white precipitate formed was filtered off, and washed with diethyl ether (30 mL). Volatiles were evaporated to afford the desired product **4** (20.9 to 21.5 g, 44.0 to 45.3 mmol) as a white solid. Yields 79–81 % (three repeated trials). Yield 80 % (mean). ^{1}H NMR ([D$_6$]DMSO, 400 MHz) δ (ppm): conform to reported data.[41]

4.2.6 *tert*-Butyl 2-{2-[(2-*tert*-Butoxy-2-oxo-ethyl)-(2-[{2-*tert*-butoxy-2-oxo-ethyl}amino]ethyl)amino]ethylamino}acetate, Compound 6b: *Attention: store at –20 °C to avoid lactamization.* A suspension of the previously prepared disulfonamido amine **4** (21.46 g, 45.32 mmol), and K_2CO_3 (23.8 g, 172.2 mmol, 3.8 equiv.) in acetonitrile (284 mL) was refluxed for 15 minutes. *tert*-Butyl 2-bromoacetate (26.5 mL, 179.5 mmol, 4.0 equiv.) was added in one portion, and the resulting mixture was further refluxed until completion of the reaction (TLC and/or MS monitoring; 3 to 5 h). The reaction was cooled to room temperature. A second portion of K_2CO_3 (25.0 g, 180.9 mmol, 4.0 equiv.) was then added, followed by the addition of thiophenol in one portion (23 mL, 225.4 mmol, 5.0 equiv.). The resulting suspension was heated at 60 °C until completion of the reaction (TLC and/or MS monitoring; 2 to 4 h). The insoluble matter was filtered off over a Celite®545 pad and washed with CH_2Cl_2. The filtrate was concentrated then purified by chromatography on silica gel (CH_2Cl_2/MeOH, 100:0 to 95:5 *v*/*v*) to give the desired compound (14–15 g, 31.4 to 33.7 mmol)) as a clear sticky orange oil. Yields 70–74 % (three repeated trials). Yield 72 % (mean). ESI-MS ($C_{22}H_{43}N_3O_6$) *m*/*z* 446.3 [M + H]$^+$. ^{1}H NMR ($CDCl_3$, 400 MHz) δ (ppm):[29] 1.44 (s, 9H, *t*Bu); 1.45 (s, 18H, *t*Bu); 2.4 (not always visible; br s, 2H, NH); 2.67 (t, 4H, *J* 6.0 Hz, CH_2CH_2N); 2.81 (t, 4H, *J* 6.0 Hz, CH_2CH_2N); 3.31 (s, 4H); 3.33 (s, 2H).

4.2.7 *tert*-Butyl 2-[3,9-Bis(2-*tert*-butoxy-2-oxo-ethyl)-12-(2-ethoxy-2-oxo-ethoxy)-3,6,9,15-tetrazabicyclo[9.3.1]pentadeca-1(14),11(15),12-trien-6-yl]acetate, Compound 7: The title compound was prepared according to our recently published protocol with slight modifications.[29]A suspension of triamino lower part **6b** (3.09 g, 6.93 mmol), pyridinic dibromide upper part **3** (2.80 g, 7.63 mmol, 1.1 equiv.), and Na_2CO_3 (2.94 g, 27.74 mmol, 4.0 equiv.) in acetonitrile (700 mL) was stirred at room temperature for 2 days. The insoluble matter was filtered off. The filtrate was concentrated then purified by chromatography on silica gel (AcOEt/MeOH, 100:0 to 90:10 *v*/*v*) to give the desired compound **7** (3.25 g, 5.00 mmol) as a beige solid. Yield 72 %. ^{1}H NMR ($CDCl_3$ + Na_2CO_3, 400 MHz)[43] δ (ppm): 1.26 (t, 3H, *J* 7.1 Hz, Et), 1.41 (s, 9H, *t*Bu), 1.46 (s, 9H, *t*Bu), 1.47 (s, 9H, *t*Bu), 1.98–2.11 (m, 2H,CH_2CH_2N), 2.14–2.24 (m, 2H, CH_2CH_2N), 2.47–2.68 (2m, 4H, CH_2CH_2N), 3.10 (AB system, 2H, *J* 17.8 Hz), 3.29–3.48 (m, 4H), 3.65–3.76 (m, 2H), 3.92 (d of AB system, *J* 14.5 Hz, 1H), 4.12 (d of AB system, 1H, *J* 15.7 Hz), 4.21 (q, 2H, *J* 7.1 Hz, Et), 4.70 (AB system, 2H, *J* 16.3 Hz), 7.19 (AB system, 2H, *J* 8.4 Hz). ^{13}C NMR ($CDCl_3$ + Na_2CO_3,100 MHz)[43] δ (ppm): 14.2, 27.9, 28.1, 53.3, 53.81, 53.85, 54.1, 56.4, 56.5, 59.5, 59.8, 61.5, 61.7, 65.6, 82.6, 82.85, 82.94, 120.5, 122.3, 147.7, 149.8, 151.1, 168.2, 173.40, 173.2, 173.6. Elemental analysis (%): calcd. for **7**•NaBr: $C_{33}H_{54}BrN_4NaO_9$ (MW 753.70): C, 52.59; H, 7.22; N, 7.43; found C, 51.70; H, 7.22; N, 7.42.

4.2.8 2-[(3,6,9-Tris(2-*tert*-butoxy-2-oxo-ethyl)-3,6,9,15-tetrazabicyclo[9.3.1]pentadeca-1(14),11(15),12-trien-12-yl)oxy]acetic Acid, Compound 8: To a solution of compound **7** (0.774 g, ≤1.19 mmol) in EtOH (10 mL), was added a 1 M aqueous solution of NaOH (1.2 mL, 1.2 mmol, ≥1 equiv.). The resulting mixture was stirred at room temperature for 1.5 hours, then concentrated to dryness. The crude product was purified by chromatography on RP18 (MeOH/H_2O, 6:4 to 10:0 *v*/*v*) to give the desired compound **8** (0.656 g, 1.02 mmol) as an off-white powder. Yield >85 %. ^{1}H NMR ($CDCl_3$, 400 MHz) δ (ppm): conform to reported data.[29] Elemental analysis (%): calculed for a mixture of the two forms: **8** (Na salt)•H_2O/**8**(CO_2H form)•H_2O in 9:1 *mol*/*mol*: $C_{31}H_{51}N_4NaO_{10}$ (90 %) + $C_{31}H_{52}N_4O_{10}$ (10 %): C, 56.37; H, 7.80; N, 8.48; Na, 3.12; found C, 54.39; H, 7.94; N, 8.79; Na, 3.14. ESI-HRMS: calcd. for ($C_{31}H_{50}N_4O_9Na^+$): *m*/*z*: 645.3470 [M + Na]$^+$, found 645.3475, error: 0.8 ppm.

4.3 Preparation of the Bimodal Probe *Gd-PCTA-Lys(ZW800–1)-OAl* Compound 15

4.3.1 Synthesis of N$^\varepsilon$-Benzyloxycarbonyl-L-lysine allyl ester H-Lys(Cbz)-OAl, Compound 11a: H-Lys(Cbz)-OH **10** was prepared following the reported procedure.,[30] Yield 80 %. Thionyl chloride (5 mL, 69 mmol, 3.8 equiv.) was added dropwise to a vigorously stirred and cooled (ice bath) suspension of H-Lys(Cbz)-OH **10** (5.020 g, 20.0 mmol) in allyl alcohol (40 mL). The resulting yellow reaction solution was subsequently heated to reflux for 24 h. The mixture was maintained in the hot bath cooled to room temperature overnight, then concentrated to dryness. The resulting oily residue was dissolved in the smallest volume of dichloromethane; slow addition of diethyl ether provoked the precipitation of white material. The first crop (3.96 g) recovered proved to be a mixture of three compounds (TLC analysis). The second crop (0.644 g, white solid) recovered was the desired product **11a** with satisfying purity. The first crop was purified by chromatography on RP18 (solid deposit, acetonitrile/H_2O, 99:1 to 97:3 *v*/*v*) to give a second portion of pure **11a** (0.995 g). Another collected fraction (1.371 g) proved to be a mixture of the desired product with the more polar side-product H-Lys-OAl **11b**. A second purification by chromatography on RP18 (solid deposit, acetonitrile/H_2O, 99:1 to 97:3 *v*/*v*) gave a third portion of pure desired product (1.01 g). Yield 46 %. ESI-MS ($C_{17}H_{24}N_2O_4$) *m*/*z* 321.2 [M + H]$^+$;^{1}H NMR (500 MHz, [D$_6$]DMSO) δ (ppm): 1.25–1.8 (m, 6H, -CH_2-(CH_2)$_3$-CH-); 2.97 (q broad, 2H, *J* 6Hz, -NH-CH_2-); 3.99 (t broad, 1H, *J* 5.8Hz, -*CH*-NH_2-); 4.68 (d, 2H, *J* 5Hz, -O-CH_2-CH-); 5.00 (s, 2H, Ph-CH_2-O-); 5.25–5.38 (2d, 2H, *J* 18Hz,

-CH=CH_2); 5.92 (m, 1H, -CH_2-C*H*=CH_2); 7.34 (m, 5H, *Ph*-CH_2-); 8.62 (s broad, 2H, -NH_2).

4.3.2 PCTA(CO_2*t*Bu)$_3$-Lys(Cbz)-OAl, Compound 12: PCTA-(CO_2*t*Bu)$_3$-COOH **11a** (101 mg, 0.157 mmol), H-Lys(Cbz)-OAl **8** (60 mg, 0.187 mmol, 1.2 equiv.), and HBTU (120 mg, 0.316 mmol, 2.0 equiv.) were placed under argon atmosphere and solubilized in anhydrous dichloromethane (2 mL). DIPEA (64 µL, 0.367 mmol, 2.3 equiv.) was then added, and the mixture was stirred at room temperature for 4 h. The organic solution was washed with water (3 × 3 mL) then concentrated to dryness to give the desired PCTA(CO_2*t*Bu)$_3$-Lys(Cbz)-OAl (53 mg) as a yellow-brown oil. Yield 38 %. ESI-MS ($C_{48}H_{72}N_6O_1$): *m/z* 925.6 [M + H]$^+$; ^{1}H NMR (500 MHz, $CDCl_3$) δ (ppm): 1.11–1.50 (m, 4H, -CH_2-CH_2-CH_2-CH_2-); 1.33–1.50 (m, 27H, -C(O)-O-*tBu*); 1.66–1.90 (m, 2H, -CH-CH_2-CH_2-); 1.91–2.16 (m, 4H, -N-CH_2-CH_2-N-); 2.34–2.57 (m, 4H, -N-CH_2-CH_2-N-); 2.94–3.12 (m, 4H, -N-CH_2-C-); 3.21–3.56 (m, 6H, N-CH_2-CO_2-); 3.72–3.90 (m, 2H, -CH_2-CH_2-NH-CO_2-); 4.00–4.10 (m, 1H, -NH-C*H*-CH_2); 4.40–4.60 (m, 2H and 2H, -CH_2-CH=CH_2 and -O-CH_2-CO-); 5.05 (s, 2H, O-CH_2-Ph); 5.20 (2 d, 2H, *J* 11Hz, -CH=CH_2); 5.83 (m, 1H, -C*H*=CH_2); 7.00 (m, 1H, -C*H*Pyr); 7.09 (m, 1H, -C*H*Pyr); 7.24 (m, 5H, -O-CH_2-*Ph*).

4.3.3 PCTA(COOH)$_3$-Lys(H)-OAl, Compound 13: PCTA(CO_2*t*Bu)$_3$-Lys(Cbz)-OAl **12** (20 mg, 21.6 µmol) was dissolved in dichloromethane (600 µL). A first portion of TFA (300 µL) was added, and the mixture was stirred at room temperature for 6 h before addition of a second portion of TFA (100 µL). Stirring was maintained for additional 3 days. The product was precipitated with diethyl ether, collected by centrifugation, washed with diethyl ether (3 × 2 mL), then dried under *vacuum* to give PCTA(COOH)$_3$-Lys(H)-OAl (10.6 mg) as a yellow-brown oil. Yield 78 %. ESI-MS ($C_{28}H_{42}N_6O_{10}$): *m/z* 623.3 [M + H]$^+$, 645.3 [M + Na]$^+$; NMR ^{1}H, 500 MHz, CD_3OD: δ (ppm) 1.18–2.05 (m, 6H, -CH-CH_2-CH_2-CH_2-); 2.93 (t, 2H, *J* 8Hz, -CH_2-NH_3^+); 3.37–4.58 (m, 8H, -C-CH_2-N-CH_2-CH_2-N-); 3.82–4.10 (3s, 6H, -N-CH_2-CO); 4.26–4.57 (m, 4H, -C-CH_2-N-CH_2-CH_2-N-); 4.66 (m broad, 1H, -NH-C*H*-CH_2-); 4.80 (d, 2H, *J* 6Hz, -CH_2-CH=CH_2); 4.9 (S, 2H, -O-CH_2-CO-); 5.31 (2d, 2H, *J* 17Hz, -CH=CH_2); 5.96 (m, 1H, -C*H*=CH_2); 7.32 (d, 1H, *J* 7Hz, -C*H*Pyr); 7.44 (d, 1H, *J* 10Hz, -C*H*Pyr).

4.3.4 Gd-PCTA-Lys(H)-OAl, Compound 14: A solution of $GdCl_3$•6H_2O (6.95 mg, 18.7 µmol, 1.1 equiv.) in water (500 µL) was added dropwise to a solution of PCTA(COOH)$_3$-Lys(H)-OAl **13** (10.6 mg, 17.0 µmol) in water (500 µL). *pH* was adjusted and maintained to 5 < *pH* < 6 with a 0.1 M aqueous solution of NaOH, and the mixture was warmed at 50 °C overnight. The presence of free Gd^{3+} was revealed by the colorimetric test with arsenazo.[42] The aqueous reaction mixture was treated with Chelex® resin, then freeze-dried to give the corresponding gadolinium complex **14** (8.6 mg) as a white powder. Yield 65 %. ESI-MS ($C_{28}H_{39}GdN_6O_{10}$): *m/z* 779.2 [M + H]$^+$, 801.2 [M + Na]$^+$.

4.3.5 Gd-PCTA-Lys(ZW800–1)-OAl, Compound 15: A solution of EDC•HCl (38.3 mg, 199.7 µmol, 8.3 equiv.) in water (300 µL) was added dropwise to a solution of Gd-PCTA-Lys(H)-OAl **14** (18.7 mg, 24.0 µmol) in water (600 µL). *pH* was controlled and maintained to 5 < *pH* < 6. A solution of ZW800–1 (18.9 mg, 0.02 mmol, 1 equiv.) in water (200 µL) was then added, and the mixture was stirred for 4 h. The solution was first dialyzed for 2 days then lyophilized. The resulting solid material was washed with dichloromethane (4 × 1.5 mL), then volatiles eliminated to give the desired probe **15** (29 mg) as a green solid. Yield 85 %. ESI-MS ($C_{79}H_{104}GdN_{10}O_{18}S_2^+$): *m/z* 851.8 [M + H]$^{2+}$.

Conflicts of interest

The authors declare no conflict of interest.

Acknowledgments

This work was performed with the financial support of the FNRS, FEDER, the ARC, the Walloon Region (Gadolymph, Holocancer and Interreg projects), the Interuniversity Attraction Poles of the Belgian Federal Science Policy Office and the COST actions. Authors thank the Center for Microscopy and Molecular Imaging (CMMI, supported by European Regional Development Fund Wallonia). Thanks to J. De Winter, PhD, and Prof. P. Gerbaux from S^{2}MOs lab for the mass spectra.

Keywords: Magnetic resonance imaging · Photoacoustic imaging · Gadolinium · Chelates · Macrocyclic ligands

[1] J. Wahsner, E. M. Gale, A. Rodriguez-Rodriguez, P. Caravan, *Chem. Rev.* **2019**, 119:957, 1057.
[2] H. S. Thomsen, S. K. Morcos, T. Almen, M.-F. Bellin, M. Bertolotto, G. Bongartz, O. Clement, P. Leander, G. Heinz-Peer, P. Reimer, F. Stacul, A. van der Molen, J. A. W. Webb, *Eur. Radiol.* **2013**, *23*, 307–318.
[3] a) E. Gianolio, P. Bardini, F. Arena, R. Stefania, E. Di Gregorio, R. Iani, S. Aime, *Radiology* **2017**, *57*, 839–849; b) A. S. Beam, K. G. Moore, S. N. Gillis, K. F. Ford, T. Gray, A. H. Steinwinder, A. Graham, *Radiol. Technol.* **2017**, *88*, 583–589; c) T. J. Fraum, D. R. Ludwig, M. R. Bashir, K. J. Fowler, *J. Magn. Reson. Imaging* **2017**, *46*, 338.
[4] B. Rosenkrantz, K. Friedman, H. Chandarana, A. Melsaether, L. Moy, Y.-S. Ding, K. Jhaveri, L. Beltran, R. Jain, *Nucl. Medicine Mol. Imaging* **2016**, *206*, 162–172.
[5] W. Sauter, H. F. Wehrl, A. Kolb, M. S. Judenhofer, B. J. Pichler, *Trends Mol. Med.* **2010**, *16*, 508–515.
[6] Louie, *Chem. Rev.* **2010**, *110*, 3146–3195.
[7] S. N. M. Chilla, C. Henoumont, L. Vander Elst, R. N. Muller, S. Laurent, *Isr. J. Chem.* **2017**, *57*, 800–808.
[8] J. L. Su, B. Wang, K. E. Wilson, C. L. Bayer, Y. S. Chen, S. Kim, K. A. Homan, S. Y. Emelianov, *Expert Opin. Med. Diagn.* **2010**, *4*, 497–510.
[9] J. Yao, L. V. Wang, *Contrast Media Mol. Imaging* **2011**, *6*, 332–345.
[10] H. S. Choi, K. Nasr, S. Alyabyev, D. Feith, J. H. Lee, S. H. Kim, Y. Ashitate, H. Hyun, G. Patonay, L. Strekowski, M. Henary, J. V. Frangioni, *Angew. Chem. Int. Ed.* **2011**, *50*, 6258–6263.
[11] a) R. Liu, L. Jing, D. Peng, Y. Li, J. Tian, Z. DAl, *Theranostics* **2015**, *5*, 1144–1153; b) L.-S. Bouchard, M. Sabieh Anwar, G. L. Liu, B. Hann, Z. H. Xie, J. W. Gray, X. Wang, A. Pines, F. F. Chen, *Proc. Natl. Acad. Sci. USA* **2009**, *106*, 4085–4089; c) H. Qin, T. Zhou, S. Yang, Q. Chen, Q. Xing, *Nanomedicine* **2013**, *8*, 1611–1624; d) M. Pob, R. J. Tower, J. Napp, L. C. Appold, T. Lammers, F. Alves, C.-C. Gluer, S. Boretius, C. Feldmann, *Chem. Mater.* **2017**, *29*, 3547–3554.
[12] H. Stetter, W. Frank, R. Mertens, *Tetrahedron* **1981**, *37*, 767–772.
[13] S. Aime, M. Botta, S. G. Crich, G. B. Giovenzana, G. Jommi, R. Pagliarin, M. Sisti, *Inorg. Chem.* **1997**, *36*, 2992–3000.
[14] W. D. Kim, G. E. Kiefer, F. Maton, K. McMillan, R. N. Muller, A. D. Sherry, *Inorg. Chem.* **1995**, *34*, 2233–2243.
[15] G. Tirsco, Z. Kovacs, A. D. Sherry, *Inorg. Chem.* **2006**, *45*, 9269–9280.
[16] E. T. Clarke, E. Martell, *Inorg. Chim. Acta* **1991**, *190*, 37–46.
[17] M. Port, I. Raynal, L. Vander Elst, R. N. Muller, F. Dioury, C. Ferroud, A. Guy, *Contrast Med. Mol. Imaging* **2006**, *1*, 121–127.
[18] S. Aime, M. Botta, S. G. Crich, G. Giovenzana, R. Pagliarin, M. Sisti, E. Terreno, *Magn. Reson. Chem.* **1998**, *36*, S200–S208.
[19] P. Fries, A. Muller, R. Seidel, P. Robert, G. Denda, M. D. Menger, G. Schneider, A. Buecker, *Invest. Radiol.* **2015**, *50*, 835–42.
[20] F. Dioury, C. Ferroud, A. Guy, M. Port, *Tetrahedron* **2009**, *65*, 7573–7579.
[21] F. Dioury, S. Sambou, E. Guéné, M. Sabatou, C. Ferroud, A. Guy, M. Port, *Tetrahedron* **2007**, *63*, 204–214.
[22] ICH GCP, Clinical Trials Registry; https://ichgcp.net/clinical-trials-registry/NCT02973516 (accessed 02 April **2019**).).
[23] Ferroud, H. Borderies, E. Lasri, A. Guy, M. Port, *Tetrahedron Lett.* **2008**, *49*, 5972–5975.
[24] G. Bort, S. Catoen, H. Borderies, A. Kebsi, S. Ballet, G. Louin, M. Port, C. Ferroud, *Eur. J. Med. Chem.* **2014**, *87*, 843–861.

[25] M. Enel, N. Leygue, N. Saffon, C. Galaup, C. Picard, *Eur. J. Org. Chem.* **2018**, *15*, 1765–1773.
[26] J. Yong-Sang, F. Dioury, V. Meneyrol, I. Ait-Arsa, J.-P. Idoumbin, F. Guibbal, J. Patché, F. Gimié, I. Khantalin, J. Couprie, P. Giraud, C. Ferroud, E. Jestin, O. Meilhac, *Eur. J. Med. Chem.* **2019**, *176*, 129–134.
[27] M. A. Baldo, G. Chessa, G. Marangoni, B. Pitteri, *Synthesis* **1987**, *8*, 720–723.
[28] R. Hovland, C. Glogard, A. J. Aasen, J. Klaveness, *Org. Biomol. Chem.* **2003**, *1*, 644–647.
[29] J. Uenishi, T. Tanaka, K. Nishiwaki, S. Wakabayashi, S. Oae, H. Tsukube, *J. Org. Chem.* **1993**, *58*, 4382–4388.
[30] Z. Balajthy, *Org. Preparations and Procedures International* **1991**, *23*, 375–376.
[31] S. Schwenk, C. Ronco, A. Oberheide, H.-D. Arndt, *Eur. J. Org. Chem.* **2016**, 4795–4799.
[32] K. Djanashvili, J. A. Peters, *Contrast Med. Mol. Imaging* **2007**, *2*, 67–71.
[33] M. Enel, N. Leygue, S. Balayssac, S. Laurent, C. Galaup, L. Vander Elst, C. Picard, *Dalton Trans.* **2017**, *46*, 4654–4668.
[34] Solomon, *Phys. Rev.* **1955**, *99*, 559–565.
[35] N. Bloembergen, *J. Chem. Phys.* **1957**, *99*, 572–573.
[36] N. Bloembergen, L. O. Morgan, *J. Chem. Phys.* **1961**, *34*, 842.
[37] Henoumont, L. Vender Elst, S. Laurent, R. N. Muller, *J. Phys. Chem.* **2010**, *114*, 3689–3697.
[38] Henoumont, L. Vander Elst, R. N. Muller, S. Laurent, Edited by Rainer Kimmich, *RSC*, **2018**, London.
[39] Guerbet, M. Port, *Lipophilic chelates and use thereof in imaging* (**2006**), WO Patent No 2006100305.
[40] S. Laurent, L. Vander Elst R. N. Muller, *Contrast Med. Mol. Imaging* **2006**, *1*, 128–137.
[41] J.-M. Siaugue, F. Segat-Dioury, I. Sylvestre, A. Favre-Réguillon, J. Foos, C. Madic, A. Guy, *Tetrahedron* **2001**, *57*, 4713–4718.
[42] Barge, G. Cravotto, E. Gianolo, F. Fedeli, *Contrast Med. Mol. Imaging* **2006**, *1*, 184–188.
[43] The NMR traces of the chromatographed fractions are variable with the presence of the two forms, NaBr adduct and free-Na form, in different proportions. Consequently, qualification (nature, purity) was preferred on samples treated to complete conversion in NaBr adduct. For that purpose, the solution in $CDCl_3$ (0.5 mL) of the chromatographed compound **7** (12.3 mg) was treated with Na_2CO_3 (10.0 mg, 94.3 µmol, *ca* 5 equiv.) and vigorously stirred for 1 day at room temperature; the NMR spectra (^1H, and ^{13}C) evolved to the characteristic traces previously reported and presented on Figure 3-S1(a)[20,23] After washings to neutrality with D_2O (3 × 1 mL), both ^1H and ^{13}C NMR spectra are quite different (Figure 3-S1(b)) and representative of that of the free-Na form with several species in equilibrium. Moreover, when a solution in $CDCl_3$ (1 mL) of the chromatographed compound **7** (25.1 mg) was treated with aluminum oxide 60 activity IV (500 mg with 50 µL of H_2O), a mixture of the two forms was obtained (Figure 3(c)).

Received: April 8, 2019

Bimodal Contrast Agents

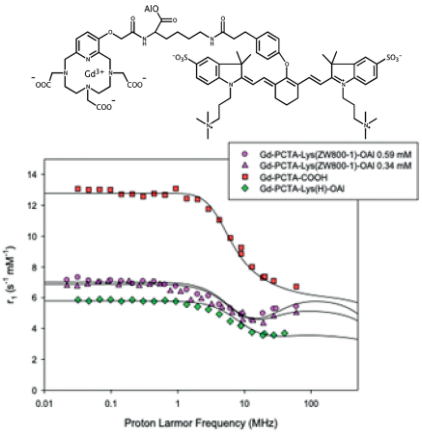

Magnetic resonance imaging (MRI) has a low sensitivity. Coupling it with a more sensitive technique like photoacoustic imaging (PAI) improves the quality of the image. The probes explored in this paper are Gd-PCTA for MRI coupled with ZW800–1 for PAI.

DOI: 10.1002/ejic.201900387